ACS Catalysis

Research Article

pubs.acs.org/acscatalysis

Removal of Nitric Oxide through Visible Light Photocatalysis by g-C_3N_4 Modified with Perylene Imides

Guohui Dong,*[,†,∥] Liping Yang,[†,‡,∥] Fu Wang,[†] Ling Zang,*[,§] and Chuanyi Wang*[,†]

[†]Laboratory of Environmental Sciences and Technology, Xinjiang Technical Institute of Physics & Chemistry, Key Laboratory of Functional Materials and Devices for Special Environments, Chinese Academy of Sciences, Urumqi 830011, People's Republic of China

[‡]The Graduate School of Chinese Academy of Science, Beijing 100049, People's Republic of China

[§]Nano Institute of Utah and Department of Materials Science and Engineering, University of Utah, Salt Lake City, Utah 84112, United States

Supporting Information

ABSTRACT: For photocatalytic removal of nitric oxide (NO), two major issues need to be addressed: incomplete oxidation of NO and deactivation of the photocatalyst. In this study, we aimed to solve these two problems by constructing an all-solid-state Z-scheme heterojunction (PI-*g*-C_3N_4) consisting of g-C_3N_4 surface modified with perylene imides (PI). PI-*g*-C_3N_4 exhibits significant enhancement in photocatalytic activity (in comparison to pristine g-C_3N_4) when examined for NO removal. More importantly, the Z-scheme charge separation within PI-*g*-C_3N_4 populates electrons and holes into the increased energy levels, thereby enabling direct reduction of O_2 to H_2O_2 and direct oxidation of NO to NO_2. H_2O_2 can further oxidize NO_2 to NO_3^- ion at a different location (via diffusion), thus alleviating the deactivation of the catalyst. The results presented may shed light on the design of visible photocatalysts with tunable reactivity for application in solar energy conversion and environmental sustainability.

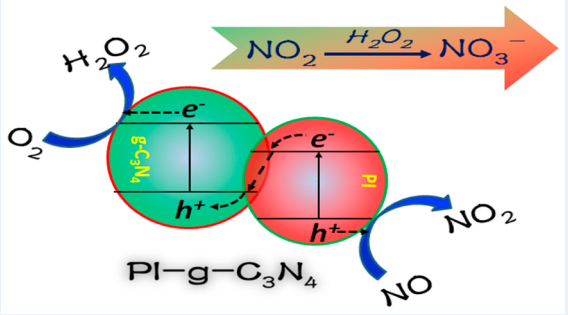

KEYWORDS: *nitric oxide removal, g-C_3N_4, Z-scheme, PTCDI, molecular oxygen activation*

INTRODUCTION

As a common gaseous pollutant, nitric oxide (NO) causes environmental problems, such as haze, photochemical smog, acid rain, and ozone depletion.[1−3] The concentration of NO in the atmosphere has greatly increased over the past decades because of the increasing numbers of automobiles and amount of industrial activities.[4,5] Therefore, developing efficient and economical technologies to eliminate atmospheric NO has become a global concern. Although some methods, including thermal catalysis reduction and physical or chemical adsorption, have been adopted to remove NO from the atmosphere, most of them suffer from low efficiency and may produce secondary pollution.[6−9] As an efficient catalytic process that can be operated under mild conditions (e.g., without high temperature or addition of strong oxidizing or reducing reagents), semiconductor photocatalysis has recently been recognized as an attractive alternative technology for NO removal.[10] Under ambient light irradiation (with energy equal to or higher than the bandgap of the semiconductor), an electron (e^-) is excited from the valence band (VB) into the conduction band (CB), leaving a hole (h^+) in the valence band. The photogenerated electrons and holes migrate to the photocatalyst surface and initiate subsequent redox reactions.[11] Through the redox reactions, NO can be eliminated effectively. Utilization of solar energy to treat environment problems, such as those via photocatalysis, has been considered to be the most energy-efficient and cost-effective approach.

It was reported that metal oxide semiconductors such as TiO_2, SiO_2, and Al_2O_3 could function as effective photocatalysts for complete removal of NO under UV light irradiation.[12−14] However, the wide band gap of these materials limits the photoresponse to the UV region, with no use of visible light, which accounts for about 5 times higher intensity in comparison to UV light in the solar spectrum. Therefore, it is desirable to develop visible light sensitive photocatalysts for their practical application in NO removal. In this regard, many visible light photocatalysts, such as BiOBr, $InVO_4$, Bi_2MoO_6, $(BiO)_2CO_3$, and graphitic carbon nitride (g-C_3N_4), have been developed and utilized for NO removal.[15−20] Among these catalysts, g-C_3N_4 is a metal-free polymeric semiconductor material, which has become increasingly promising for photocatalysis under visible light mainly due to its desirable band gap of 2.7 eV, strong robustness, and low cost.[21−23] Our previous work demonstrated that g-C_3N_4 could oxidize NO to

Received: June 12, 2016
Revised: August 2, 2016
Published: August 24, 2016

DOI: 10.1021/acscatal.6b01657
ACS Catal. 2016, 6, 6511−6519

Scheme 1. Synthetic Route of PI-*g*-C_3N_4

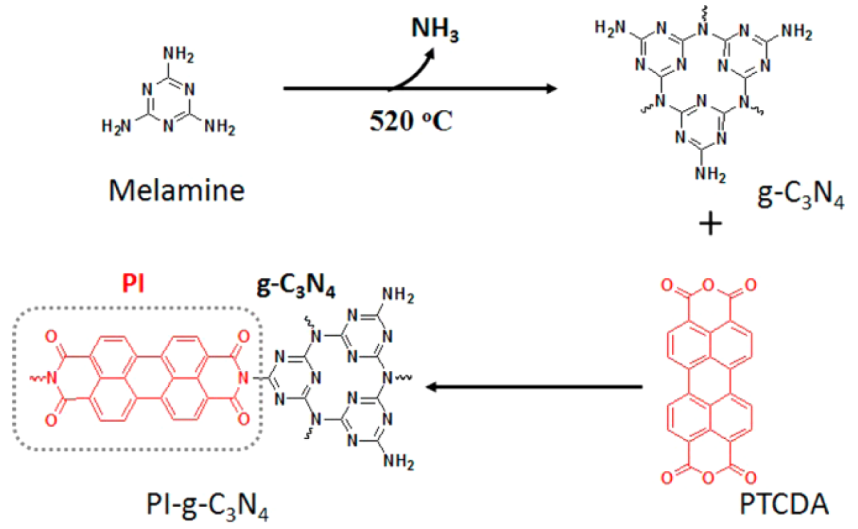

NO_2 under visible light irradiation.[24] However, NO_2 is a more toxic gas, which is detrimental to the lungs and increases the risk of bronchitis and pulmonary fibrosis. Recently, we found that modification of g-C_3N_4 with noble metals could change the photocatalytic reaction of NO from producing NO_2 to NO_3^-.[25] However, NO_3^- ions occupy the surface active sites and cause deactivation of the catalyst. Therefore, it is of the utmost interest, though a great challenge, to design a modification method which causes g-C_3N_4 to deeply oxidize NO to NO_3^- but with minimal deactivation in catalytic activity. In nature, photosynthesis with a Z-scheme charge transfer process can separate the photogenerated electrons and holes into two photosystems through an electron mediator.[26] Inspired by the advantages of photosynthesis, we aimed to design an all-solid-state Z-scheme heterojunction structured photocatalyst based on g-C_3N_4, with which the photogenerated electrons and holes can be separated into two different phases, helping spatially isolate the oxidation and reduction reaction sites[26] and thus minimizing the catalytic deactivation.

Molecules of perylene tetracarboxylic diimide (PTCDI) represent a unique class of n-type organic semiconductor, with strong thermal and light stability.[27] PTCDI materials have been extensively used in bulk heterojunction (BHJ) solar cells because of their strong visible light absorption, good charge transportation properties, and durable photostability.[27−29] PTCDI can be synthesized through a one-step reaction between perylene tetracarboxylic dianhydride (PTCDA) and a primary amine ($-NH_2$). Since the edges of g-C_3N_4 are full of $-NH_2$ groups, PTCDI can be modified onto g-C_3N_4 simply by reacting PTCDA with g-C_3N_4 in solution. In this study, we provide an all-solid-state Z-scheme heterojunction consisting of PI and g-C_3N_4 (PI-*g*-C_3N_4) for the photocatalytic removal of NO under visible light. The structure of the PI-*g*-C_3N_4 heterojunction was characterized by various experimental methods. In comparison to the single-phase g-C_3N_4, PI-*g*-C_3N_4 demonstrated much improved photocatalytic efficiency for NO removal. The photocatalysis mechanism of the heterojunction structure was deeply explored, as presented below.

EXPERIMENTAL SECTION

Preparation of Photocatalysts. All chemicals were purchased in analytical grade and used without further purification. g-C_3N_4 was synthesized by direct heating of melamine following a protocol developed in our previous work.[30] Typically, a given amount of melamine was placed in a covered crucible and heated to 520 °C at a heating rate of 20 °C/min and kept at 520 °C for 4 h.

In order to modify the surface of g-C_3N_4 with PTCDI, PTCDA was chosen to react with g-C_3N_4 via the condensation reaction illustrated in Scheme 1. Briefly, PTCDA (0.0355 g), g-C_3N_4 (0.71 g), and imidazole (2.5 g) were placed in a 100 mL three-neck round-bottom flask, followed by heating at 140 °C for 5 h under a nitrogen atmosphere. Then the reaction mixture was cooled to room temperature and 50 mL of ethanol was placed in the reaction vessel with stirring. The solution was then transferred to a 250 mL flask containing 150 mL of 2 M hydrochloric acid (HCl). After it was stirred for 12 h, the mixture was centrifuged and washed thoroughly with methanol and deionized water. The resulting red solid was transferred to a 100 mL round-bottom flask containing 50 mL of potassium carbonate aqueous solution (K_2CO_3, 10%), which was refluxed in an oil bath at 100 °C for 1 h. After it was cooled to 50 °C, the solution was centrifuged and washed three times with 300 mL of K_2CO_3 solution (10%) and then with 50 mL of 2 M HCl (2 mol/L). The sample obtained was finally washed thoroughly with methanol and deionized water until the pH of the rinsed water became neutral. The collected solids (PI-*g*-C_3N_4) were dried under vacuum at 80 °C for 12 h.

Sample Characterization. UV−vis absorption spectra of g-C_3N_4 and PI-g-C_3N_4 were recorded on a Solid Spec-3700 DUV spectrophotometer using $BaSO_4$ as reference and were converted from reflection to absorption by the Kubelka−Munk method. The powder X-ray diffraction (XRD) measurements were recorded on a Bruker D8 diffractometer with monochromated Cu Kα radiation (λ = 1.5418 Å). Fluorescence spectra were monitored with a fluorescence spectrophotometer (Hitachi, Model F-7000) equipped with a PC recorder. Electron paramagnetic resonance (EPR) spectra were recorded on a Bruker ElexsysE500 spectrometer by applying an X-band (9.43 GHz, 1.5 mW) microwave with sweeping magnetic field at 110 K in cells that can be connected to a conventional high-

DOI: 10.1021/acscatal.6b01657
ACS Catal. 2016, 6, 6511−6519

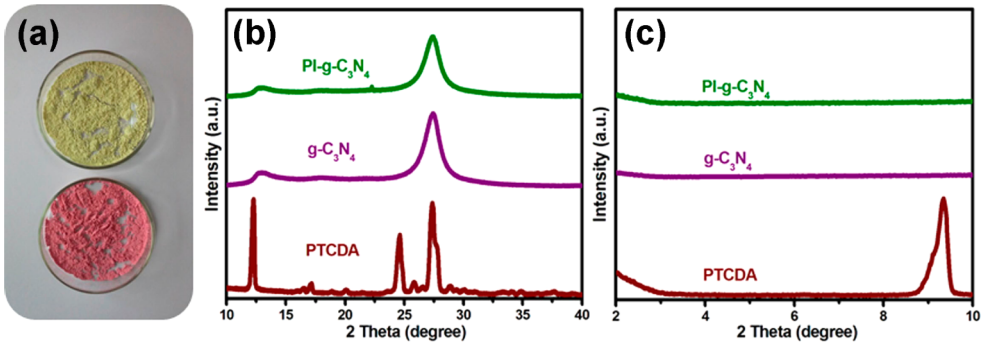

Figure 1. (a) Photographs of g-C_3N_4 (yellow) and PI-*g*-C_3N_4 (pink) solid showing the different colors. (b) XRD patterns of PI-*g*-C_3N_4, g-C_3N_4 ,and PTCDA. (c) Small-angle XRD patterns of PI-*g*-C_3N_4, g-C_3N_4, and PTCDA.

vacuum apparatus (residual pressure $<10^{-4}$ mbar). Surface electronic states were analyzed by an X-ray photoelectron spectrometer (XPS, ESCALAB MK II). All binding energies were calibrated by using the contaminant carbon (C(1s) = 284.6 eV) as a reference. Transmission electron microscopy (TEM) imaging was performed on a JEOL JSM-2010 microscope. For TEM measurements, the samples were suspended in ethanol, and then a drop of this suspension was deposited onto a carbon film supported by a copper grid.

Photocatalytic NO Removal Test. Photocatalytic removal of NO was tested over g-C_3N_4, PI-*g*-C_3N_4, or PTCDA under visible or UV light irradiation. The experiments were performed at ambient temperature in a continuous-flow reactor with a starting concentration of NO at 600 ppb levels. A cylindrical reactor with a volume of 0.785 L ($\pi R^2 H$ ($\pi \times 5^2$ cm^2 $\times$ 10 cm)) was made of Pyrex glass with a top window made of quartz. A glass dish (R = 3 cm) deposited with a given amount of g-C_3N_4, PI-*g*-C_3N_4, or PTCDA was placed in the middle of the reactor. A 300 W Xe lamp with a 420 nm cutoff filter was vertically placed above the quartz window, so that the incident light can irradiate directly on the sample dish.

The glass dish samples were prepared by coating an aqueous suspension of g-C_3N_4, PI-*g*-C_3N_4, or PTCDA onto the dish. Typically, 50 mg of g-C_3N_4, PI-*g*-C_3N_4, or PTCDA was added to 10 mL of H_2O and ultrasonicated for 15 min. The aqueous suspension was then cast onto the glass dish, followed by drying at 60 °C until the water was completely removed.

During photocatalytic removal tests, the NO concentration was diluted to about 600 ppb by air stream. The flow rate was controlled at 1 L/min by a mass flow controller. The change in NO concentration was continuously measured by using a chemiluminescence NO analyzer (Thermo Scientific, 42i).

NO removal efficiency (η) was calculated as follows:

$$\eta\ (\%) = (1 - C/C_0) \times 100$$

where C and C_0 are the concentrations of NO in the outlet stream and feeding stream, respectively.

Scavenging Experiments. In general, photocatalytic reactions involve various active species, such as the photogenerated electron (e^-), hole (h^+), superoxide ($^\bullet O_2^-$), and hydrogen peroxide (H_2O_2). Comparative investigations of the effect of these species on the photocatalysis were performed by using scavenger agents to remove the different species. Potassium iodide (KI), potassium dichromate ($K_2Cr_2O_7$), and *tert*-butyl alcohol (TBA) were employed as scavengers for h^+, e^- and $^\bullet OH$, respectively. Typically, 50 mg of photocatalyst was mixed with 1 mM of the different trapping agents in 10 mL of H_2O and ultrasonicated for 15 min. Then, the aqueous suspensions were coated onto the glass dish followed by drying at 60 °C until the water was completely removed. The coated dishes were used in the photocatalytic NO removal experiments as described above.

Detection of H_2O_2. The concentration of H_2O_2 was determined by utilizing a fluorescence reagent, as reported in our previous work.[31] Typically, the fluorescence reagent was prepared by mixing (*p*-hydroxyphenyl)acetic acid (POHPAA, 2.7 mg) and horseradish peroxidase (1 mg) in potassium hydrogen phthalate buffer solution (10 mL, 8.2 g/L, pH 4.01) with stirring. Photocatalytic reactions (H_2O_2 generation reactions) were conducted with a 50 mL suspension containing 50 mg of the respective catalyst under visible irradiation under atmosphere (1 atm) at 20 °C. In the process of the reaction, continuous stirring was applied to keep the photocatalysts well suspended. About 2 mL of the reaction mixture was taken from the reaction cell at given time intervals and centrifuged to remove the photocatalysts. The clear solution thus obtained was added 50 μL of the fluorescence reagent. After 10 min of reaction, 1 mL of 0.1 M NaOH solution was added for the subsequent fluorescence measurements. The reaction product between H_2O_2 and the fluorescence reagent has a strong fluorescent emission at 409 nm on excitation at 315 nm.

Photoelectrochemical Experiments. The photoelectrodes were prepared according to our previously reported method.[32] Photocatalysts were dispersed in α-naphthol (0.5 wt %) solution and ground for 10 min. The resultant slurry was then blade coated on a 1× 1 cm^2 fluorine tin oxide (FTO) glass substrate with a glass slide, using adhesive tapes as spaces. Then the film was dried in air and annealed at 150 °C for 15 min. Photoelectrochemical experiments were performed in a conventional three-electrode cell with a platinum plate (1 × 1 cm^2) as the counter electrode and a saturated calomel electrode (SCE) as the reference electrode on an electrochemical workstation (CHI660C, Chenhua, People's Republic of China). The prepared working electrode was positioned in the middle of a 0.1 M KCl aqueous solution with the glass side facing the incident light. A 200 W Xe lamp with a 420 nm cutoff filter was chosen as the visible light source.

RESULTS AND DISCUSSION

After the synthesis of g-C_3N_4 and PI-*g*-C_3N_4, we found that the modification with PTCDI changes the color of g-C_3N_4 from light yellow to pink (Figure 1a), implying increased absorption in visible light. The structure of PI-*g*-C_3N_4 was characterized by X-ray diffraction (XRD) in comparison with pure g-C_3N_4 and

DOI: 10.1021/acscatal.6b01657
ACS Catal. 2016, 6, 6511−6519

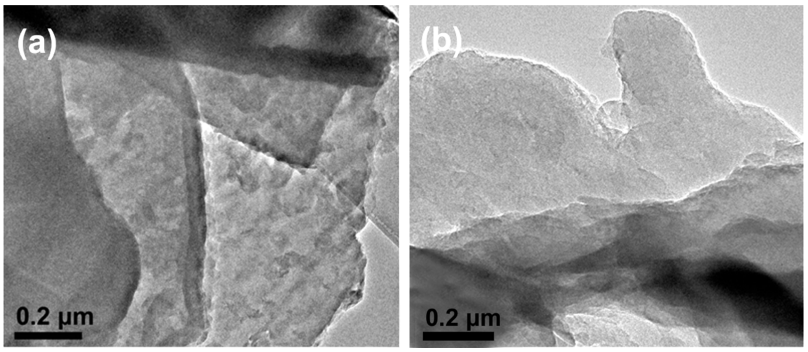

Figure 2. TEM images of g-C_3N_4 (a) and PI-*g*-C_3N_4 (b).

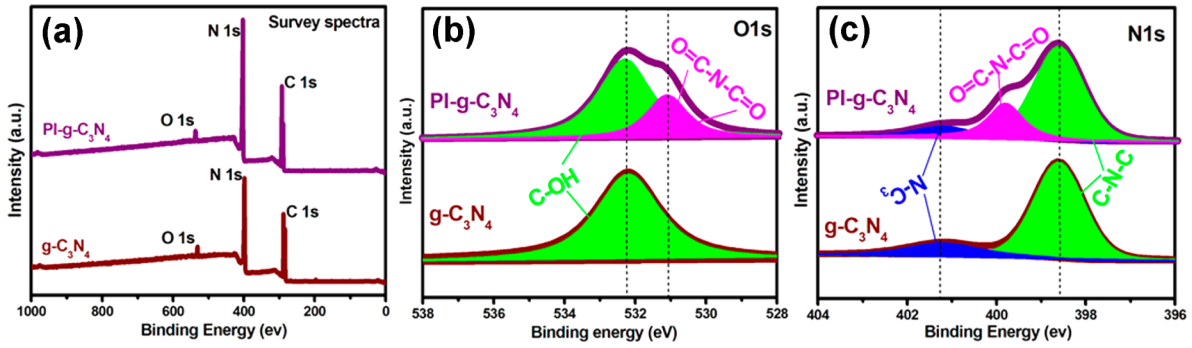

Figure 3. (a) XPS spectra of g-C_3N_4 and PI-*g*-C_3N_4. (b, c) High-resolution XPS spectra of O 1s (b) and N 1s (c) of g-C_3N_4 and PI-*g*-C_3N_4.

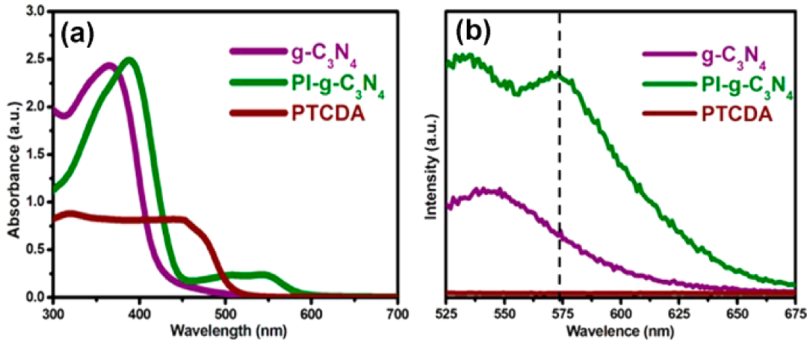

Figure 4. (a) UV−vis absorption spectra of g-C_3N_4, PI-*g*-C_3N_4, and PTCDA. (b) Photoluminescence (PL) spectra of g-C_3N_4, PI-*g*-C_3N_4, and PTCDA (excited at 500 nm).

PTCDA powders. The XRD spectra (Figure 1b,c) showed only the phase of g-C_3N_4, whereas no diffraction of the PTCDI phase was observed, indicating that the PTCDI molecules are sparsely distributed on the surface of g-C_3N_4 rather than existing as solid $\pi-\pi$ stacks. This is consistent with the low density of $-NH_2$ groups distributed along the edge of g-C_3N_4. The overall platelet-like morphology of g-C_3N_4 remained about the same after the surface modification of PTCDI, as evidenced by the transmission electron microscopy (TEM) imaging (Figure 2a,b).

XPS was further employed to investigate the surface chemical composition and chemical states of the g-C_3N_4 and PI-*g*-C_3N_4 samples (Figure 3), wherein only carbon, nitrogen, and oxygen species were detected (Figure 3a). Both of the samples show an O 1s peak at 532.2 eV, which is likely due to the surface-adsorbed H_2O or hydroxyl group. In comparison, the PI-*g*-C_3N_4 samples show a new O 1s peak at 531.1 eV (Figure 3b), which can be fitted with C−O and carbonyl groups, indicating the formation of imide groups of PTCDI. The high-resolution N 1s spectrum of g-C_3N_4 is shown in Figure 3c. The observed peak can be deconvoluted into two peaks which are ascribed to the nitrogen in C−N−C (398.4 eV) and C−N_3 (400.7 eV) groups, respectively. These two nitrogen peaks are also obtained for PI-*g*-C_3N_4 sample, indicating that the main skeleton of g-C_3N_4 remained unchanged after modification of PTCDI. Interestingly, an additional N 1s peak at 399.8 eV was observed for PI-*g*-C_3N_4, which can be attributed to the imide nitrogen within the PTCDI part.

Modification of PTCDI extended the absorption of g-C_3N_4 in the visible region, as evidenced by the emerging absorption bands around 500 and 550 nm (Figure 4a), which are characteristic of PTCDI in the solid state.[27] Moreover, the UV−vis absorption edges of PI-*g*-C_3N_4 show a red shift in comparison with that of g-C_3N_4. This phenomenon suggests that the intermolecular interaction occurs between PTCDI and g-C_3N_4. PTCDA material is not fluorescent due to the strong $\pi-\pi$ stacking, which limits the low-energy excitonic transition. PTCDI becomes fluorescent when the side groups help tune

DOI: 10.1021/acscatal.6b01657
ACS Catal. 2016, 6, 6511−6519

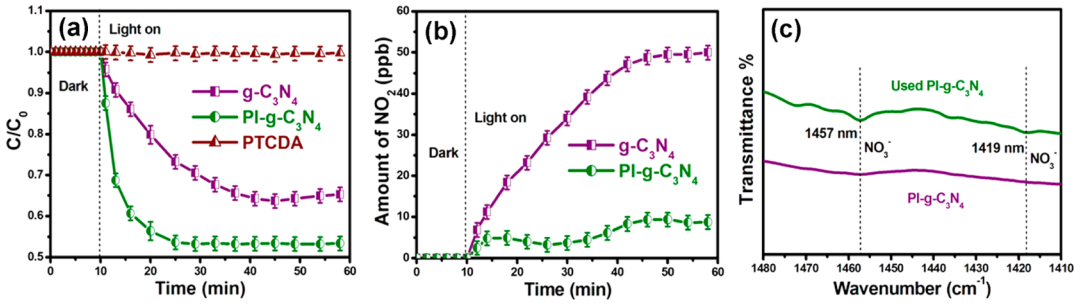

Figure 5. (a) Relative change in NO concentration (C/C_0) as a function of irradiation time tested over g-C_3N_4, PI-*g*-C_3N_4, and PTCDA. (b) NO_2 concentration changing with irradiation time tested over g-C_3N_4 and PI-*g*-C_3N_4. (c) FTIR spectra of PI-*g*-C_3N_4 before and after use in the photocatalytic removal of NO. In all of the experiments, the initial concentration of NO was 600 ppb, the amount of g-C_3N_4, PI-*g*-C_3N_4, and PTCDA used was 50 mg, and a 300 W Xe lamp with a 420 nm cutoff filter was used as the visible light source.

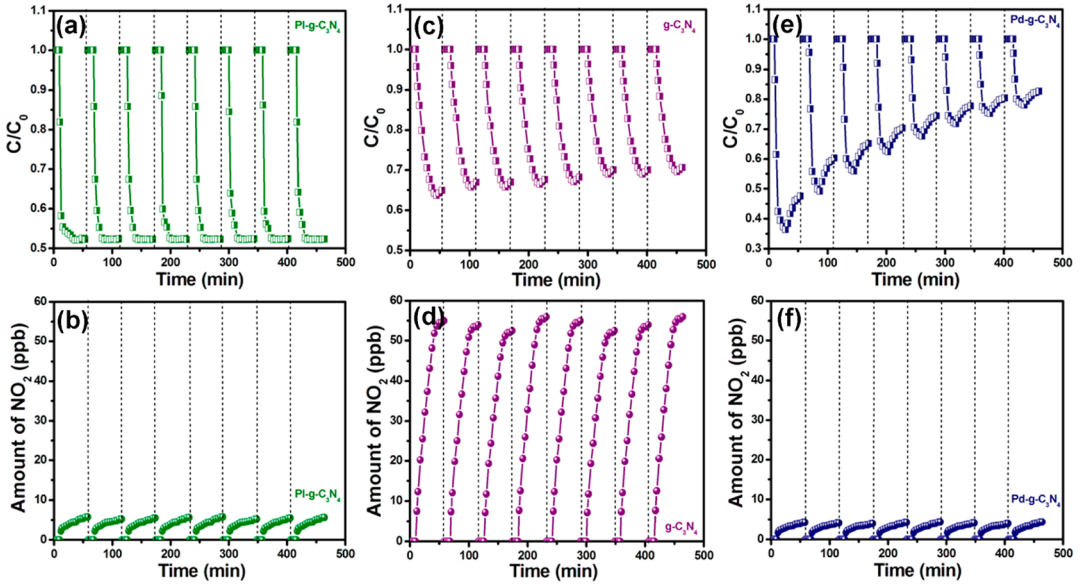

Figure 6. Repeated testing of the photocatalytic NO removal over PI-*g*-C_3N_4 (a), g-C_3N_4 (c), and Pd-*g*-C_3N_4 (e) and NO_2 concentration changes on repeated testing over PI-*g*-C_3N_4 (b), g-C_3N_4 (d), and Pd-*g*-C_3N_4 (f).

the $\pi-\pi$ stacking.[27] As shown in Figure 4b, significant fluorescence (peak at 571 nm) was observed for PI-*g*-C_3N_4 on excitation at 500 nm, indicating the existence of PTCDI, whereas the same fluorescence peak was not measured for g-C_3N_4 or PTCDA. These observations further confirm the surface modification of g-C_3N_4 by PTCDI, consistent with the XPS results above.

The as-prepared PI-*g*-C_3N_4 was employed for photocatalytic removal of NO under visible light irradiation (λ >420 nm) to investigate the effect of the heterojunction between PTCDI and g-C_3N_4 on the catalysis efficiency. Figure 5a shows the relative change of NO concentration (C/C_0) as a function of irradiation time tested over the three different catalysts PI-*g*-C_3N_4, g-C_3N_4, and PTCDA. As a control test, the removal of NO was negligible under the same visible light irradiation for 50 min, indicating the high photostability of NO to visible light. As shown in Figure 5a, 37% of the NO was removed over pure g-C_3N_4 after 35 min of irradiation, while 47% was removed in only 10 min when PI-*g*-C_3N_4 was used as a catalyst under the same irradiation, indicating much improved catalysis efficiency. (We selected an optimal relative content ratio of PI to g-C_3N_4 in the present work. The photoactivities for NO removal of samples at other ratios can be found in Figure S1 in the Supporting Information.) In contrast, PTCDA did not demonstrate any catalysis for NO removal under the same photoirradiation.

In addition to the decrease in NO concentration, the concentration of NO_2 produced during the photocatalysis was also monitored (Figure 5c). With g-C_3N_4 as the catalyst the amount of NO_2 produced increased gradually and reached a plateau value after about 40 min of irradiation, clearly indicating that the main product of the photocatalysis is NO_2. In sharp comparison, when PI-*g*-C_3N_4 was used as catalyst instead, the generation of NO_2 quickly reached its equilibrium (within ca. 5 min) and the accumulated amount of NO_2 was 1 order of magnitude lower than that in the case of g-C_3N_4. This implies that most of NO_2 was further converted (oxidized) to NO_3^-. Such conversion was confirmed by FTIR spectral measurements. The PI-*g*-C_3N_4 sample after photocatalytic tests was collected and analyzed by FTIR. It can be seen that the used PI-*g*-C_3N_4 exhibits new bands at 1457 and 1419 cm^{-1} (Figure 5d), which are ascribed to the antisymmetric stretching vibration modes of NO_3^- groups, implying that the major product in PI-*g*-C_3N_4 is NO_3^-. It was reported that NO_3^- can occupy the surface active sites, causing the deactivation of g-C_3N_4.[17,25] Therefore, the stability and recyclability of PI-*g*-C_3N_4 were examined and compared with those of g-C_3N_4 and Pd-*g*-C_3N_4 (g-C_3N_4 was modified by the nanopalladium. The main product

DOI: 10.1021/acscatal.6b01657
ACS Catal. 2016, 6, 6511−6519

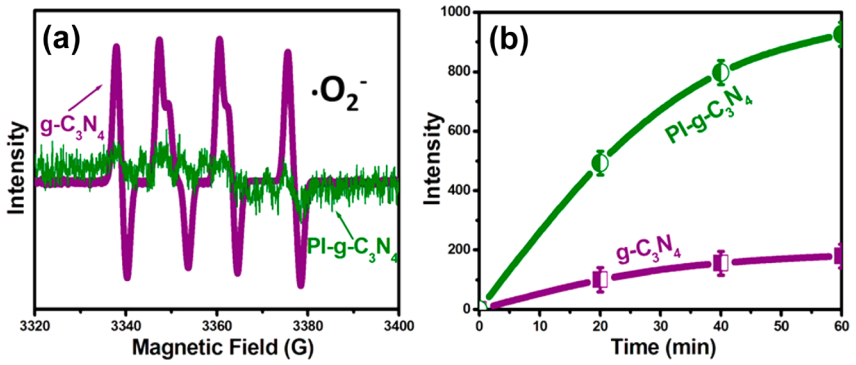

Figure 7. (a) DMPO spin-trapping ESR spectra recorded for $^{\bullet}O_2^-$ in the g-C_3N_4 and PI-*g*-C_3N_4 systems (under λ >420 nm irradiation), where the concentration of DMPO was 25 mmol L^{-1}. (b) Comparison of H_2O_2 generation in the g-C_3N_4 and PI-*g*-C_3N_4 systems under the same photocatalytic conditions.

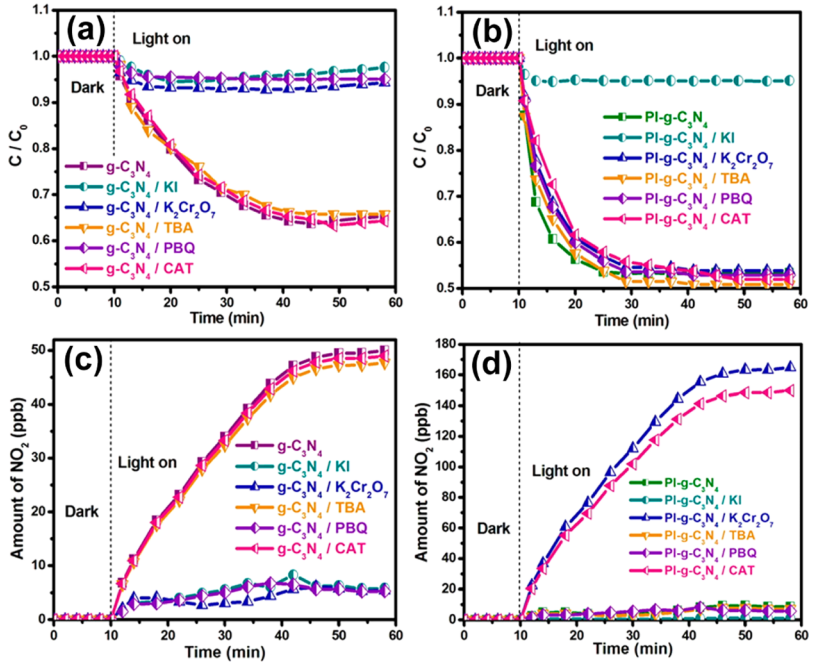

Figure 8. Influence of different scavengers (KI for h^+, $K_2Cr_2O_7$ for e^-, TBA for $^{\bullet}OH$, PBQ for $^{\bullet}O_2^-$, CAT for H_2O_2) on the photocatalytic removal of NO using g-C_3N_4 and PI-*g*-C_3N_4. The photocatalysis conditions are the same as in Figure 5.

of NO removal over it is NO_3^-.[25] The synthetic process can be found in the Supporting Information.) by running the same photocatalytic removal experiment continuously in multiple cycles. The results evince that the activity of PI-*g*-C_3N_4 does not decline after eight cycles of NO removal under the visible light irradiation (Figure 6a). However, the NO removal on g-C_3N_4 and Pd-*g*-C_3N_4 decreased about 10% and 67%, respectively (Figure 6c,e). The activity decrease of g-C_3N_4 and Pd-*g*-C_3N_4 should be attributed to the occupation of active sites caused by the NO_3^-. Although the activity of g-C_3N_4 did not significantly decline, it could produce a large amount of NO_2 in each cycle of photocatalytic NO removal (Figure 6d). In comparison with g-C_3N_4 and Pd-*g*-C_3N_4, PI-*g*-C_3N_4 can not only greatly alleviate the deactivation of NO removal but also effectively inhibit the second pollution due to the production of NO_2. The catalytic activity of PI-*g*-C_3N_4 remained about the same after eight cycles of test, indicating that the formation of NO_3^- may occur at a position segregated from the catalyst.

Generally, the photocatalytic removal of NO involves the surface reactions of both photogenerated holes and electrons, which may also produce oxidizing species, such as $^{\bullet}O_2^-$, H_2O_2 and $^{\bullet}OH$ to further the oxidation reactions.[10,33] In this study, a DMPO spin-trapping ESR technique was employed to characterize the $^{\bullet}O_2^-$ species generated during photocatalysis. As shown in Figure 7a, four characteristic peaks of DMPO-$^{\bullet}O_2^-$ were clearly observed in methanol suspensions of g-C_3N_4, whereas only a trace level of DMPO-$^{\bullet}O_2^-$ could be detected for the PI-*g*-C_3N_4 under the same conditions. However, the PI-*g*-C_3N_4 system produced about 5 times more H_2O_2 than the g-C_3N_4 system (Figure 7b). Since in semiconductor photocatalysis H_2O_2 is normally generated through direct reduction ($O_2 \rightarrow H_2O_2$) or a multistep reaction ($O_2 \rightarrow {}^{\bullet}O_2^- \rightarrow H_2O_2$) from oxygen,[31] the ESR results suggest that H_2O_2 is likely produced via direct reduction in the PI-*g*-C_3N_4 suspension, in comparison to the multistep reaction route in g-C_3N_4.

The photocatalytic reactions of NO removal over g-C_3N_4 and PI-*g*-C_3N_4 were further explored through a series of control experiments. With addition of potassium iodide (KI, a hole scavenger[34]) the NO removal was significantly depressed for both g-C_3N_4 and PI-*g*-C_3N_4 (Figure 8a,b), suggesting that the

DOI: 10.1021/acscatal.6b01657
ACS Catal. 2016, 6, 6511−6519

Scheme 2. Two Models of Charge Separation Proposed for PI-*g*-C_3N_4 under Visible Irradiation: (a) Conventional Donor–Acceptor Charge Transfer and (b) Z-Scheme Electron Transfer[a]

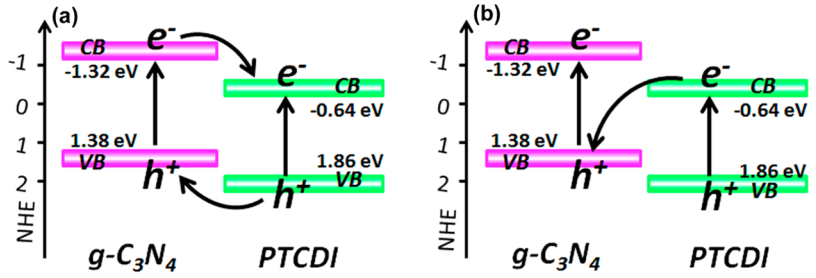

[a]Energy levels (vs NHE) are obtained from the flat potential (CB) measured in this study and the band gap values reported in the literature (see Figure 9).

photogenerated holes paly a critical role in NO removal in both cases. On the other hand, when potassium dichromate ($K_2Cr_2O_7$, an electron scavenger[35]) was added, the NO removal was inhibited over g-C_3N_4 (Figure 8a), whereas the NO removal over PI-*g*-C_3N_4 remained little changed. These observations imply that photogenerated electrons are indispensable for NO removal over g-C_3N_4 but not PI-*g*-C_3N_4. Moreover, the production of NO_2 during photocatalysis of PI-*g*-C_3N_4 was significantly increased in the presence of $K_2Cr_2O_7$ (Figure 8d), indicating that the photogenerated holes (increased due to scavenging of electrons) are primarily responsible for oxidizing NO to NO_2 in the PI-*g*-C_3N_4 system. Considering the fact that conduction band electrons can be captured by O_2 to produce active oxygen species, it is essential to explore the role of these species in conversion of NO. Comparative investigations were performed by using varying scavengers such as *tert*-butyl alcohol (TBA) for $^{\bullet}OH$,[36] *p*-benzoquinone (PBQ) for $^{\bullet}O_2^-$[37] and catalase (CAT) for H_2O_2[38] in the photocatalysis. As shown in Figure 8a,b, the addition of TBA did not change the NO removal rate over either g-C_3N_4 or PI-*g*-C_3N_4, suggesting no significant contribution from $^{\bullet}OH$ to the photocatalytic removal of NO. Addition of PBQ clearly depressed the NO removal on g-C_3N_4 (Figure 8a), but not PI-*g*-C_3N_4 (Figure 8b), implying different roles of $^{\bullet}O_2^-$ in the two systems. Also clearly seen from Figure 8 is that the addition of CAT did not affect the NO removal rate over either g-C_3N_4 or PI-*g*-C_3N_4. On the other hand, the presence of CAT dramatically increased the NO_2 concentration in the PI-*g*-C_3N_4 system (Figure 8d) but brought little effect on NO_2 generation over g-C_3N_4 (Figure 8c). These results indicate that H_2O_2 facilitates the further conversion (oxidation) of NO_2 to NO_3^- in the PI-*g*-C_3N_4 system. On the basis of these comparative observations, we conclude that both the photogenerated hole and H_2O_2 are indispensable, playing synergic roles, in the NO removal over PI-*g*-C_3N_4, enabling ultimate conversion to NO_3^- ion, whereas for the NO removal over g-C_3N_4 the synergic roles are played by the hole and $^{\bullet}O_2^-$, resulting in conversion of NO to NO_2 (consistent with the previous observation on g-C_3N_4[24]).

From the comparative investigations above, the photocatalytic removal of NO over PI-*g*-C_3N_4 may involve eqs 1–4

$$\text{PI-}g\text{-}C_3N_4 + \text{visible light} \rightarrow h^+ + e^- \quad (1)$$

$$2h^+ + NO + H_2O \rightarrow NO_2 + 2H^+ \quad (2)$$

$$e^- + O_2 + 2H^+ \rightarrow H_2O_2 \quad (3)$$

$$2NO_2 + H_2O_2 \rightarrow 2NO_3^- + 2H^+ \quad (4)$$

The efficiency of visible light photocatalysis depends on the visible light absorption of the catalyst. As shown in Figure 4a, PI-*g*-C_3N_4 (in comparison to g-C_3N_4) has increased absorption in the visible region, particularly above 500 nm, which is solely due to the absorption by the PTCDI part. This increased visible absorption caused significant enhancement in photocatalytic removal of NO, as shown in Figure 5. Such enhancement could be explained in two possible ways: one is localized on the PTCDI part, and the other is a cooperative process involving both g-C_3N_4 and PTCDI parts (Scheme 2). For the first case, visible excitation of the PTCDI (band gap 2.5 eV, see the caption of Figure 9) produces electrons and holes, which then initiate the surface redox reactions as observed for other semiconductor photocatalysts. However, the efficiency of this catalysis is limited by the fast charge recombination process, which is actually evidenced by the strong fluorescence of PTCDI measured from the PI-*g*-C_3N_4 sample (Figure 4b).

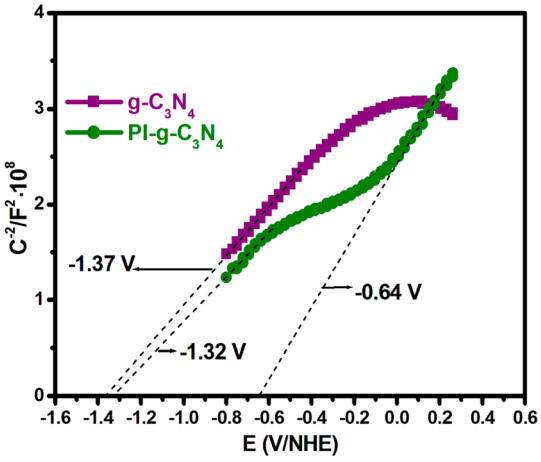

Figure 9. Mott–Schottky plots for g-C_3N_4 and PI-*g*-C_3N_4 at frequency of 1 k Hz obtained in darkness. Both g-C_3N_4 and PI-*g*-C_3N_4 samples display n-type semiconductor characteristics. The flat-band potential (equal to CB band in n-type semiconductor) was measured at −1.37 eV vs NHE for pure g-C_3N_4 and −1.32 eV vs NHE for the g-C_3N_4 part in PI-*g*-C_3N_4. With the known band gap of 2.7 eV for g-C_3N_4,[20] the VB potential of g-C_3N_4 can be calculated to be 1.38 eV vs NHE in the PI-*g*-C_3N_4 composite. The second linear region in the Mott–Schottky plot of PI-*g*-C_3N_4 is attributed to the CB band of the PTCDI part, corresponding to a potential of −0.64 eV vs NHE. With the known band gap of 2.5 eV for PTCDI,[24] the VB potential of PTCDI can be calculated to be 1.86 V vs NHE.

DOI: 10.1021/acscatal.6b01657
ACS Catal. 2016, 6, 6511–6519

PTCDI alone is unlikely to afford the high efficiency of visible photocatalysis. Thereby, the cooperative process (Scheme 2) becomes the reasonable interpretation for the observed enhancement in visible photocatalysis.

As shown in Scheme 2 (the band potentials were acquired from the Mott–Schottky plots, Figure 9), both the g-C_3N_4 and PTCDI parts are excited under visible light (λ >420 nm), followed by electron transfer between g-C_3N_4 and PTCDI, which can be classified into two models. The first is the common donor–acceptor charge separation as illustrated in Scheme 2a, in which electron transfer occurs from the CB of g-C_3N_4 to the CB of PTCDI, leaving a hole in the VB of g-C_3N_4. If the charge migration occurs via this model, the enhancement of photocatalytic NO removal should also be observed under the UV-light illumination (λ <400 nm). The absorption coefficient of PTCDI in the UV region is about 15 times lower than the maximum in the region of 500–550 nm (also note that for PTCDI the absorption coefficient does not change with different side substitutions[39]). From the UV–vis absorption spectrum measured for the PI-*g*-C_3N_4 sample in this study (Figure 4a), the absorption of the PTCDI part in the UV region should be 15 times lower than the maximum peak in the region of 500–550 nm (where g-C_3N_4 has no absorption). By carefully examining the absorption data, we can conclude that the absorption of PI-*g*-C_3N_4 in the UV region is truly dominated by the absorption by g-C_3N_4 (>99% in absorption coefficient). That is to say, under UV irradiation (λ <400 nm) only the g-C_3N_4 part is excited. After the excitation, photogenerated electrons will transfer from the CB of g-C_3N_4 to the CB of PTCDI, producing electrons and holes located at the PTCDI and g-C_3N_4, respectively, the same charge separation as illustrated in Scheme 2a. However, as shown in Figure 10, under UV irradiation the photocatalytic removal of

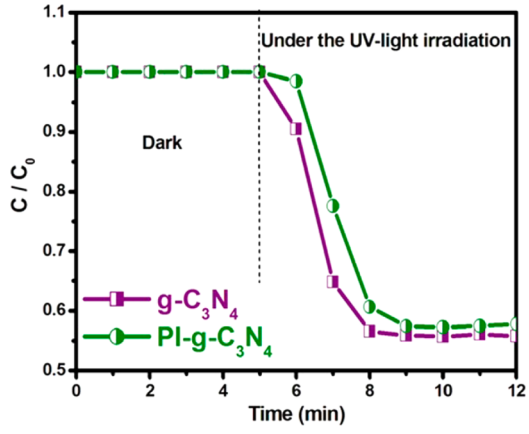

Figure 10. Photocatalytic removal of NO under UV light irradiation (λ <400 nm). For UV irradiation (λ <400 nm), more than 99% of the irradiation will be absorbed by the g-C_3N_4 part.

NO on PI-*g*-C_3N_4 was even slower than that on g-C_3N_4. This observation suggests that the common charge separation model shown in Scheme 2a is not likely the case in the visible photocatalysis of PI-*g*-C_3N_4. The second model is the Z-scheme charge migration (Scheme 2b), for which the visible excitation initiates the electron transfer from the CB of PTCDI to the VB of g-C_3N_4. This results in a different way of charge separation with an electron located in the CB of g-C_3N_4 and a hole in the VB of PTCDI.[40] The lower level of VB of PTCDI (by 0.48 eV in comparison to that of g-C_3N_4) provides stronger oxidizing power for the hole, thus enabling direct oxidation of NO to NO_2 (eq 2), which is consistent with the results shown in Figure 5 as discussed above. Meanwhile the electron located in the CB of g-C_3N_4 possesses higher reducing power (by 0.68 eV in comparison to that of PTCDI), thereby enabling direct reduction of O_2 to H_2O_2 (eq 3), which is also consistent with the results presented in Figures 7 and 8. Because the NO_2, H_2O_2, and NO_3^- species are formed at different sites in the PI-*g*-C_3N_4 system, the deactivation of catalysis caused by the occupation of active sites could be alleviated greatly (Scheme 3). The heterojunction charge separation as illustrated by the

Scheme 3. NO Photocatalytic Mechanism of PI-*g*-C_3N_4 under Visible Light Irradiation

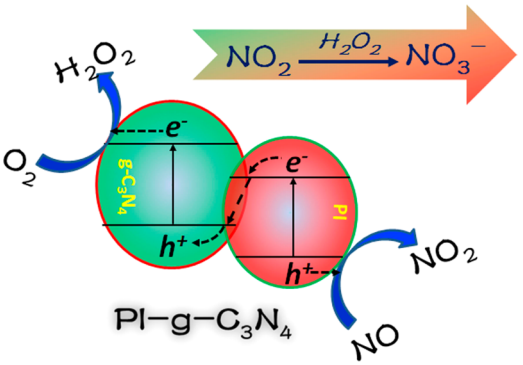

Z-scheme reduces the probability of charge recombination that is often encountered in the single-component photocatalyst, thus producing an increased density of holes and electrons, which can act as charge carriers when the catalyst material is employed in a circuit. This is evidenced by the results shown in Figure 11, wherein the photocurrent generated over PI-*g*-C_3N_4 (4.6 μA cm^{-2}) was about 15 times higher than that over g-C_3N_4 (0.3 μA cm^{-2}).

CONCLUSIONS

In summary, an all-solid-state Z-scheme heterojunction (PI-*g*-C_3N_4) has been successfully constructed. As tested for photocatalytic removal of NO under visible light, significant

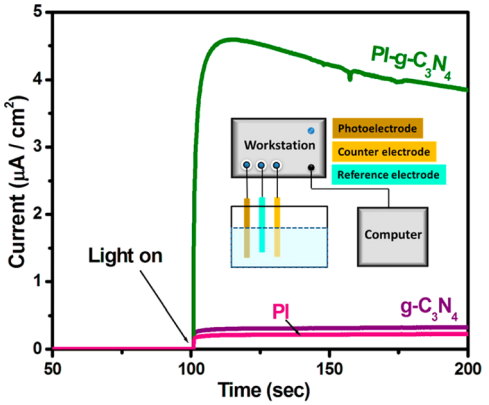

Figure 11. Photocurrent–time curves of g-C_3N_4 and PI-*g*-C_3N_4 electrodes in 0.1 M KCl aqueous solution under visible light irradiation (λ >420 nm). For comparison, the photocurrent–time curve of PI was also detected under the same conditions. PI was prepared in the same manner as for PI-*g*-C_3N_4, but g-C_3N_4 was replaced by melamine.

DOI: 10.1021/acscatal.6b01657
ACS Catal. 2016, 6, 6511–6519

enhancement in catalytic activity was observed for PI-g-C_3N_4 in comparison to the pristine g-C_3N_4. The Z-scheme heterojunction creates charge separation with the electron populated to the higher CB and hole to the lower VB, thus enhancing the redox reaction power of the charge carriers. The strong hole can directly oxidize NO to NO_2, while the strong electron can directly reduce O_2 to H_2O_2. Since NO_2 and H_2O_2 can react at different locations (via diffusion), the NO_3^- ion produced would cause minimal deactivation to the catalyst. This study provides new insight into the design of effective photocatalysts that can be operated under visible light, facilitating the utilization of solar energy.

■ ASSOCIATED CONTENT

Supporting Information

The Supporting Information is available free of charge on the ACS Publications website at DOI: 10.1021/acscatal.6b01657.

Details of the preparation of Pd-g-C_3N_4 and the photoactivities for NO removal of other samples which have different content ratios of PI to g-C_3N_4 (PDF)

■ AUTHOR INFORMATION

Corresponding Authors

*G.D.: e-mail, donggh@ms.xjb.ac.cn; tel, +86-0991-3835879; fax, +86-0991-3838957.

*L.Z.: e-mail, lzang@eng.utah.edu.

*C.W.: e-mail, cywang@ms.xjb.ac.cn.

Author Contributions

‖These authors contributed equally to this work.

Notes

The authors declare no competing financial interest.

■ ACKNOWLEDGMENTS

Financial support by the National Nature Science Foundation of China (Grant No. 21473248), the CAS/SAFEA International Partnership Program for Creative Research Teams, the CAS "Western Light" program (2015-XBQN-B-06), and the NSF (CBET 1502433) is gratefully appreciated.

■ REFERENCES

(1) Lerdan, M. T.; Munger, J. W.; Jacob, D. J. *Science* **2000**, *289*, 2291−2293.

(2) Takahashi, K. *Chem. Commun.* **2015**, *51*, 4062−4064.

(3) Rodriguez, J. A.; Jirsak, T.; Liu, G.; Hrbek, J.; Dvorak, J.; Maiti, A. *J. Am. Chem. Soc.* **2001**, *123*, 9597−9605.

(4) Kreuzer, L. B.; Patel, C. K. N. *Science* **1971**, *173*, 45−47.

(5) Kim, C. H.; Qi, G. S.; Dahlberg, K.; Li, W. *Science* **2010**, *327*, 1624−1627.

(6) Shelef, M. *Chem. Rev.* **1995**, *95*, 209−225.

(7) Yu, J. J.; Jiang, Z.; Zhu, L.; Hao, Z. P.; Xu, Z. P. *J. Phys. Chem. B* **2006**, *110*, 4291−4300.

(8) Xiao, B.; Wheatley, P. S.; Zhao, X. B.; Fletcher, A. J.; Fox, S.; Rossi, A. G.; Megson, L. L.; Bardiga, S.; Regli, L.; Thomas, K. M.; Morris, R. E. *J. Am. Chem. Soc.* **2007**, *129*, 1203−1209.

(9) Ma, L.; Li, J. H.; Ke, R.; Fu, L. X. *J. Phys. Chem. C* **2011**, *115*, 7603−7612.

(10) Ai, Z. H.; Ho, W. K.; Lee, S. C.; Zhang, L. Z. *Environ. Sci. Technol.* **2009**, *43*, 4143−4150.

(11) Linsebigler, A. L.; Lu, G. Q.; Yates, J. T. *Chem. Rev.* **1995**, *95*, 735−758.

(12) Takeuchi, M.; Yamashita, H.; Matsuoka, M.; Anpo, M.; Hitao, T.; Iton, N. *Catal. Lett.* **2000**, *67*, 135−137.

(13) Liu, Z. M.; Ma, L. L.; Junaid, A. S. M. *J. Phys. Chem. C* **2010**, *114*, 4445−4450.

(14) Anpo, M.; Shioya, Y.; Yamashita, H.; Giamello, E.; Morterra, C.; Che, H.; Webber, S.; Ouellette, S. *J. Phys. Chem.* **1994**, *98*, 5744−5750.

(15) Ai, Z. H.; Ho, W. K.; Lee, S. C. *J. Phys. Chem. C* **2011**, *115*, 25330−25337.

(16) Dong, F.; Ho, W. K.; Lee, S. C.; Wu, Z. B.; Fu, M.; Zou, S. C.; Huang, Y. *J. Mater. Chem.* **2011**, *21*, 12428−12436.

(17) Ding, X.; Ho, W. K.; Shang, J.; Zhang, L. Z. *Appl. Catal., B* **2016**, *182*, 316−325.

(18) Ai, Z. H.; Zhang, L. Z.; Lee, S. C. *J. Phys. Chem. C* **2010**, *114*, 18594−18600.

(19) Ma, J. Z.; Wang, C. X.; He, H. *Appl. Catal., B* **2016**, *184*, 28−34.

(20) Huang, H. W.; Li, X. W.; Wang, J. J.; Dong, F.; Chu, P. K.; Zhang, T. R.; Zhang, Y. H. *ACS Catal.* **2015**, *5*, 4094−4103.

(21) Wang, X. C.; Maeda, K.; Thomas, A.; Takanabe, K.; Xin, G.; Carlsson, J. M.; Domen, K.; Antonietti, M. *Nat. Mater.* **2009**, *8*, 76−80.

(22) Xiong, T.; Cen, W. L.; Zhang, Y. X.; Dong, F. *ACS Catal.* **2016**, *6*, 2462−2472.

(23) Dong, F.; Zhao, Z. W.; Sun, Y. J.; Zhang, Y. X.; Yan, S.; Wu, Z. B. *Environ. Sci. Technol.* **2015**, *49*, 12432−12440.

(24) Dong, G. H.; Ho, W. K.; Zhang, L. Z. *Appl. Catal., B* **2015**, *174*−*175*, 477−485.

(25) Li, Y. H.; Yang, L. P.; Dong, G. H.; Ho, W. K. *Molecules* **2016**, *21*, 36.

(26) Zhou, P.; Yu, J. G.; Jaroniec, M. *Adv. Mater.* **2014**, *26*, 4920−4935.

(27) Chen, S.; Slattum, P.; Wang, C. Y.; Zang, L. *Chem. Rev.* **2015**, *115*, 11967−11998.

(28) Zang, L. *Acc. Chem. Res.* **2015**, *48*, 2705−2714.

(29) Hains, A. W.; Liang, Z. Q.; Woodhouse, M. A.; Gregg, B. A. *Chem. Rev.* **2010**, *110*, 6689−6735.

(30) Dong, G. H.; Zhang, L. Z. *J. Phys. Chem. C* **2013**, *117*, 4062−4068.

(31) Li, S. N.; Dong, G. H.; Hailili, R.; Yang, L. P.; Li, Y. X.; Wang, F.; Zeng, Y. B.; Wang, C. Y. *Appl. Catal., B* **2016**, *190*, 26−35.

(32) Dong, G. H.; Ho, W. K.; Wang, C. Y. *J. Mater. Chem. A* **2015**, *3*, 23435−23441.

(33) Dong, F.; Wang, Z. Y.; Li, Y. H.; Ho, W. K.; Lee, S. C. *Environ. Sci. Technol.* **2014**, *48*, 10345−10353.

(34) Wang, Z. J.; Ghasimi, S.; Landfester, K.; Zhang, K. A. I. *Adv. Mater.* **2015**, *27*, 6265−6270.

(35) Wang, L.; Jiang, X. Z. *Environ. Sci. Technol.* **2008**, *42*, 8492−8497.

(36) Yan, S. C.; Li, Z. S.; Zou, Z. G. *Langmuir* **2010**, *26*, 3894−3910.

(37) Zhang, T. T.; Lei, W. Y.; Liu, P.; Rodriguez, J. A.; Yu, J. G.; Qi, Y.; Liu, G.; Liu, M. H. *J. Phys. Chem. C* **2016**, *120*, 2777−2786.

(38) Wang, L.; Cao, M. H.; Ai, Z. H.; Zhang, L. Z. *Environ. Sci. Technol.* **2014**, *48*, 3354−3362.

(39) Zang, L.; Che, Y. K.; Moore, J. S. *Acc. Chem. Res.* **2008**, *41*, 1596−1608.

(40) Cheng, H. J.; Hou, J. G.; Takeda, O.; Guo, X. M.; Zhu, H. M. *J. Mater. Chem. A* **2015**, *3*, 11006−11013.

DOI: 10.1021/acscatal.6b01657
ACS Catal. 2016, 6, 6511−6519